Nano-Hexapod on top of a Spindle - Test Bench

Dehaeze Thomas

March 19, 2024

Contents

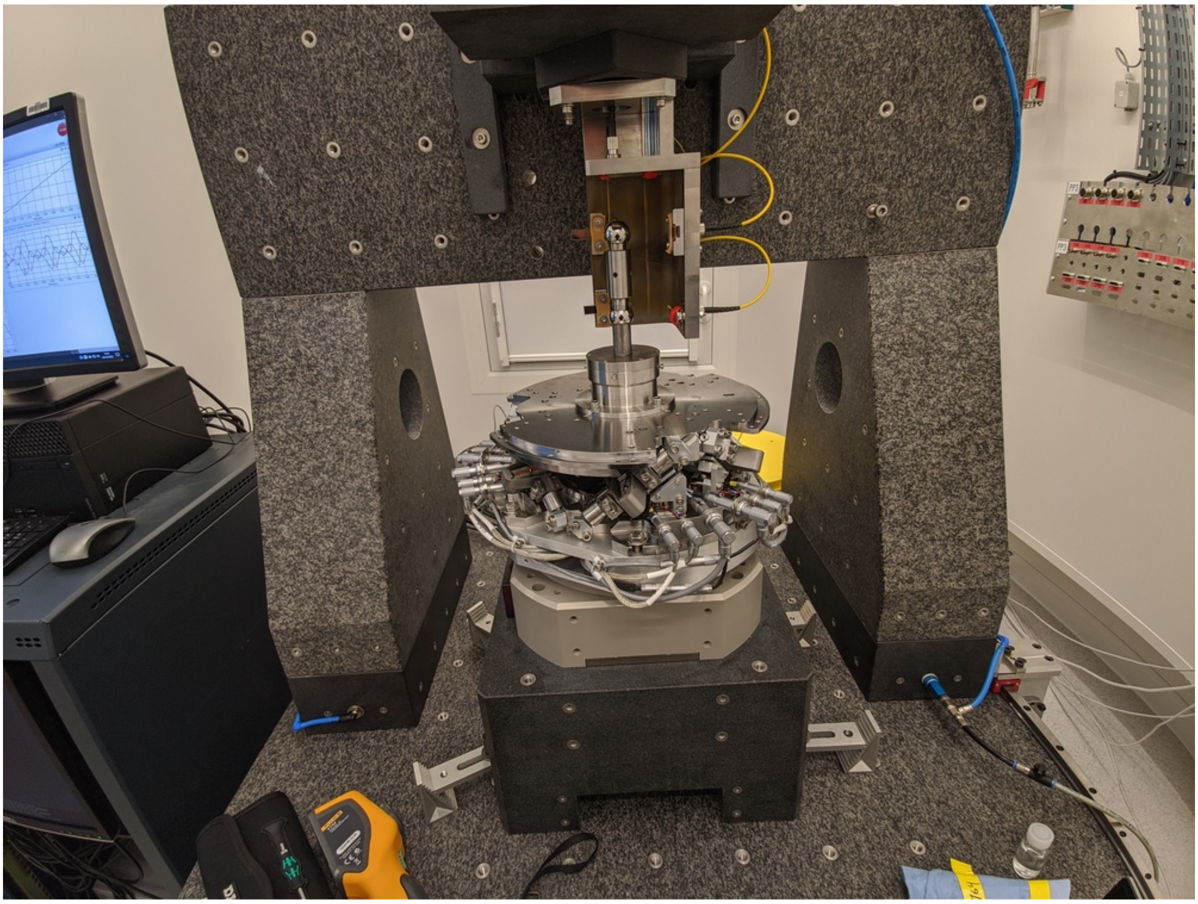

Figure 1: Setup with the Spindle, nano-hexapod and metrology

1 Test-Bench Description

Note

Here are the documentation of the equipment used for this test bench:

- Voltage Amplifier: PiezoDrive PD200
- Amplified Piezoelectric Actuator: Cedrat APA300ML
- DAC/ADC: Speedgoat IO131
- Encoder: Renishaw Vionic and used Ruler
- LION Precision CPL290
- Spindle: Lab Motion RT250S with Drivebox 3.6 controller

1.1 Alignment

Procedure:

1. Align bottom sphere with the spindle rotation axis (~ 10um)
2. Align top sphere with the spindle rotation axis (~ 10um)

1.2 Short Range metrology system

There are 5 interferometers pointing at 2 spheres as shown in Figure 1.2.

	Value
Sphere Diameter	25.4mm
Distance between the spheres	76.2mm

Assumptions:

- Interferometers are perfectly positioned / oriented
- Sphere is perfect

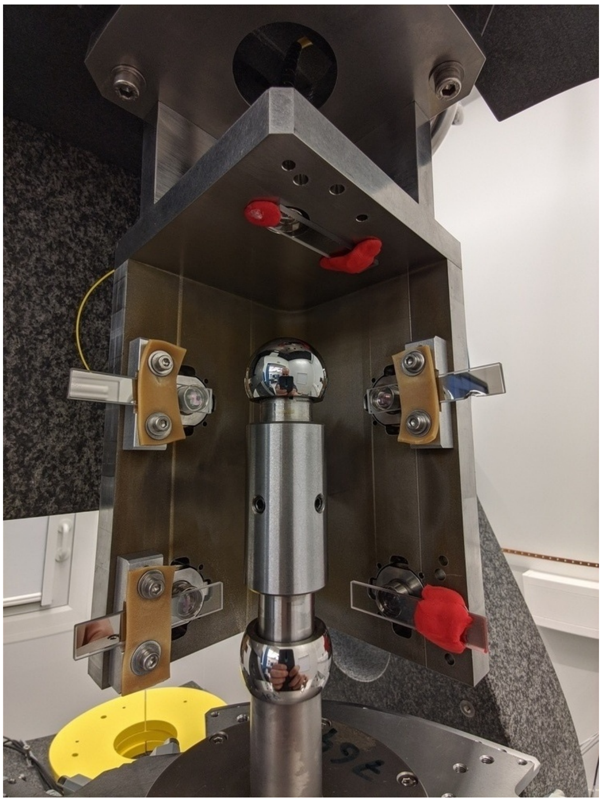

Figure 1.1: Metrology system with LION sphere (1 inch diameter) and 5 interferometers fixed to their individual tip-tilts

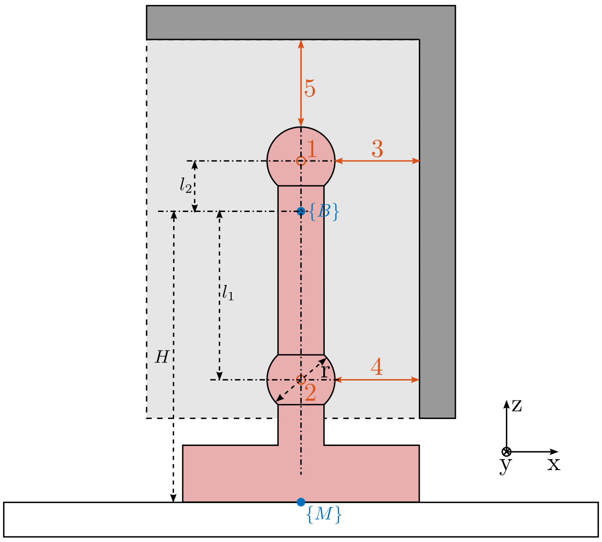

Figure 1.2: Schematic of the measurement system

Compute the Jacobian matrix:

- From pure X-Y-Z-Rx-Ry small motions, compute the effect on the 5 measured distances
- Compute the matrix
- Inverse the matrix
- Verify that it is working with simple example (for example using Solidworkds)

We have the following set of equations:

$$d_1 = -D_y + l_2 R_x \tag{1.1}$$
$$d_2 = -D_y - l_1 R_x \tag{1.2}$$
$$d_3 = -D_x - l_2 R_y \tag{1.3}$$
$$d_4 = -D_x + l_1 R_y \tag{1.4}$$
$$d_5 = -D_z \tag{1.5}$$

That can be written as a linear transformation:

$$\begin{bmatrix} d_1 \\ d_2 \\ d_3 \\ d_4 \\ d_5 \end{bmatrix} = \begin{bmatrix} 0 & -1 & 0 & l_2 & 0 \\ 0 & -1 & 0 & -l_1 & 0 \\ -1 & 0 & 0 & 0 & -l_2 \\ -1 & 0 & 0 & 0 & l_1 \\ 0 & 0 & -1 & 0 & 0 \end{bmatrix} \cdot \begin{bmatrix} D_x \\ D_y \\ D_z \\ R_x \\ R_y \end{bmatrix} \tag{1.6}$$

By inverting the matrix, we obtain the Jacobian relation:

$$\begin{bmatrix} D_x \\ D_y \\ D_z \\ R_x \\ R_y \end{bmatrix} = \begin{bmatrix} 0 & -1 & 0 & l_2 & 0 \\ 0 & -1 & 0 & -l_1 & 0 \\ -1 & 0 & 0 & 0 & -l_2 \\ -1 & 0 & 0 & 0 & l_1 \\ 0 & 0 & -1 & 0 & 0 \end{bmatrix}^{-1} \cdot \begin{bmatrix} d_1 \\ d_2 \\ d_3 \\ d_4 \\ d_5 \end{bmatrix} \tag{1.7}$$

Table 1.1: Jacobian matrix for the metrology system

	d1	**d2**	**d3**	**d4**	**d5**
Dx	0.0	0.0	-0.79	-0.21	0.0
Dy	-0.79	-0.21	-0.0	-0.0	0.0
Dz	0.0	0.0	0.0	0.0	-1.0
Rx	13.12	-13.12	0.0	-0.0	0.0
Ry	0.0	0.0	-13.12	13.12	0.0

1.3 Spindle errors

The spindle is rotated at 60rpm during 10 turns. The signal of all 5 interferometers are recorded.

1.3.1 Errors in D_x and D_y

Because of the eccentricity of the reference surfaces (the spheres), we expect the motion in the X-Y plane to be a circle as a first approximation. We can first see that in Figure 1.3 that shows the measured D_x and D_y motion as a function of the R_z angle.

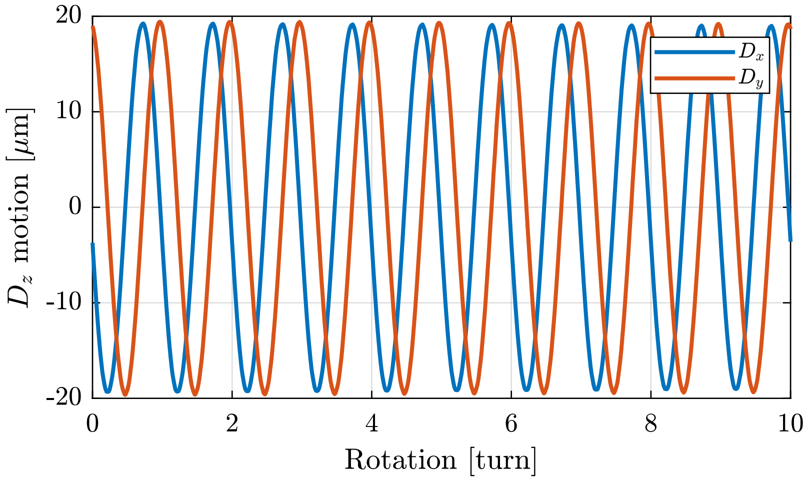

Figure 1.3: Dx and Dy motion during the rotation

A circle is fit, and the obtained radius of the circle (i.e. the excentricity) is estimated to be:

```
Results
Error linked to excentricity = 19 um
```

The motion in the X-Y plane as well as the circle fit and the residual motion (circle fit subtracted from the measured motion) are shown in Figure 1.4.

Let's now analyse the frequency content in the signal.

1.3.2 Errors in vertical motion D_z

The top interferometer is measuring the vertical motion of the sphere.

However, if the top sphere is not perfectly aligned with the spindle axis, there will also measure some vertical motion due to this excentricity.

Let's fit a sinus with a period of one turn.

```
Results
Errors linked to excentricity = 410 [nm]
```

If we look at the remaining motion after removing the effect of the eccentricity (Figure 1.8, right), we can see a signal with 20 periods every turn. Let's fit this.

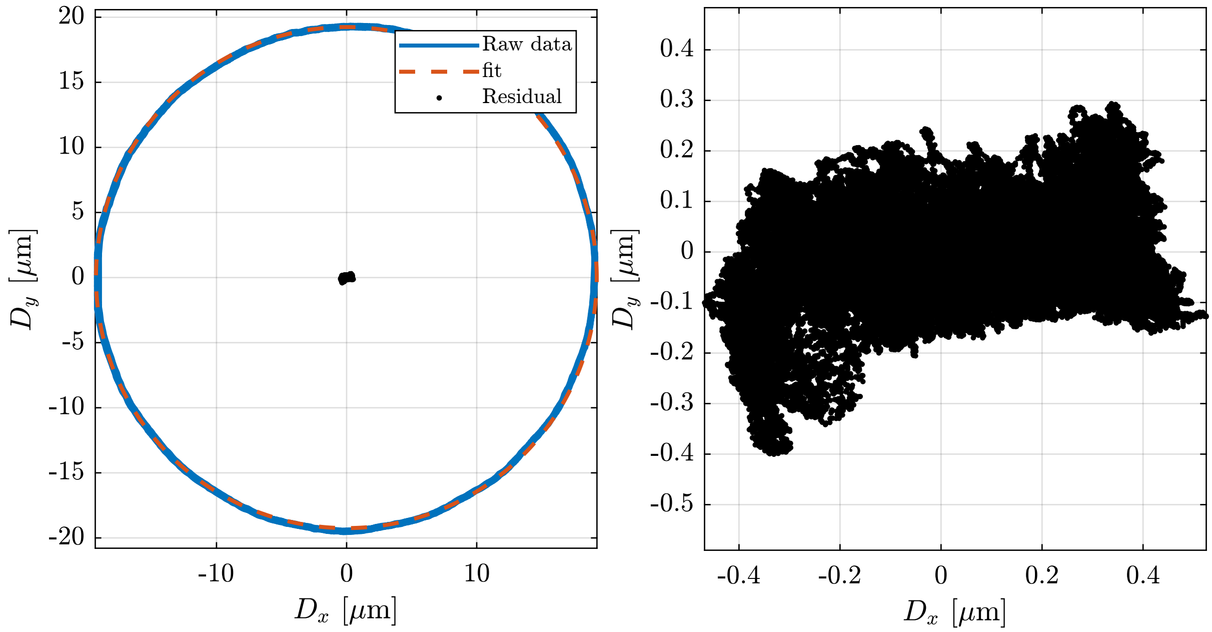

Figure 1.4: Dx and Dy motion during the spindle rotation

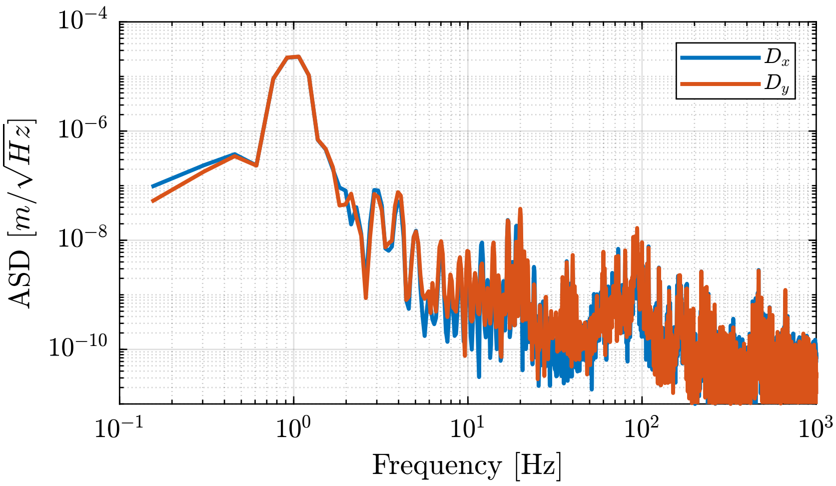

Figure 1.5: Amplitude Spectral Density of the measured Dx and Dy motion

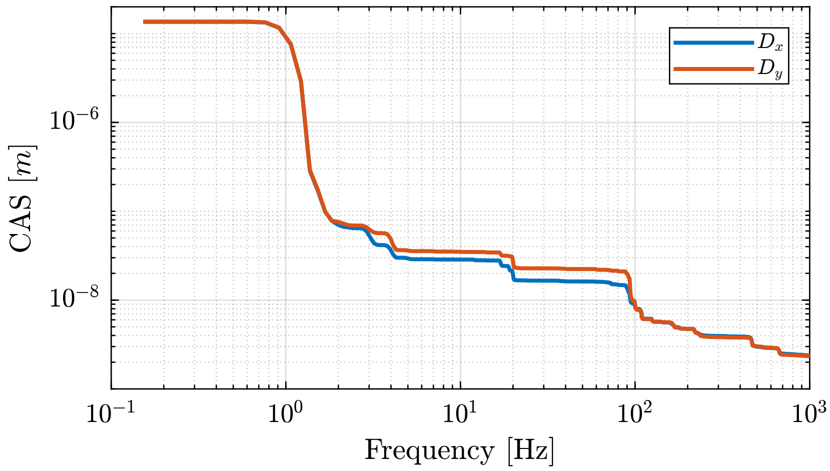

Figure 1.6: Cumulative Amplitude Spectrum of the measured Dx and Dy motion

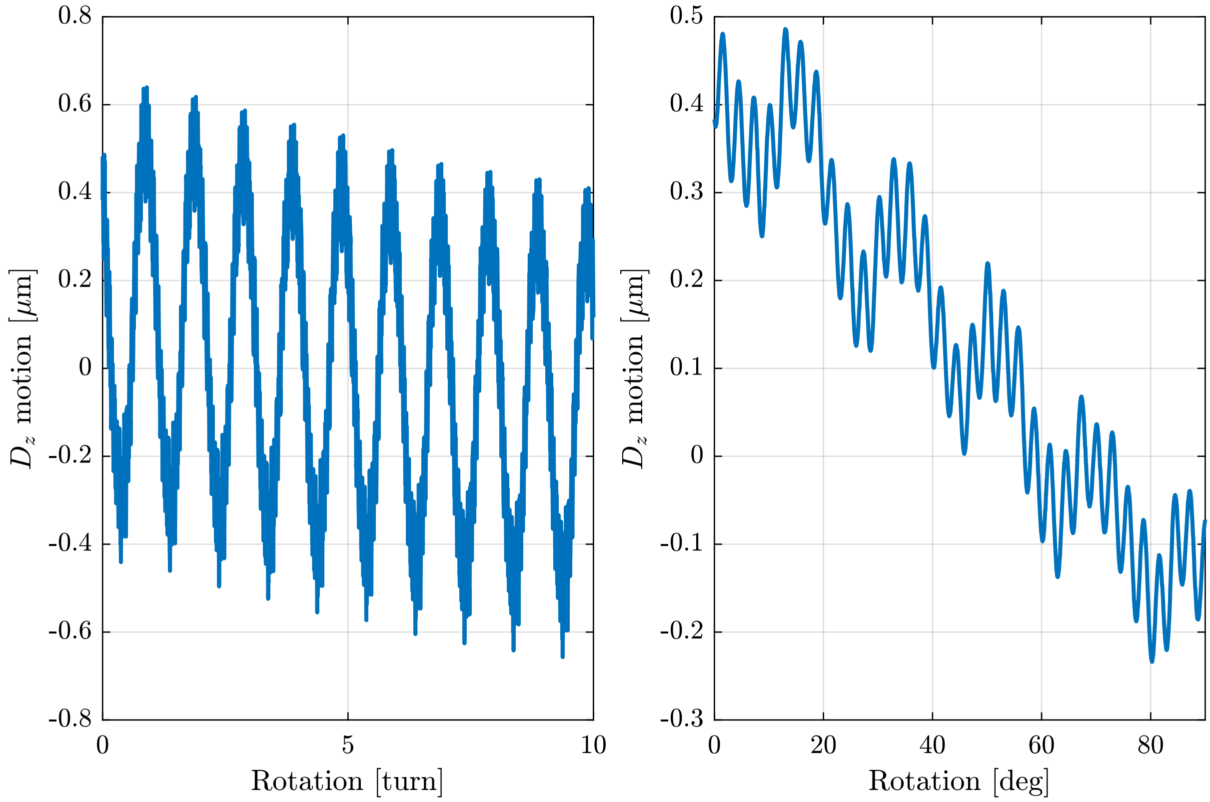

Figure 1.7: Dz motion during the rotation

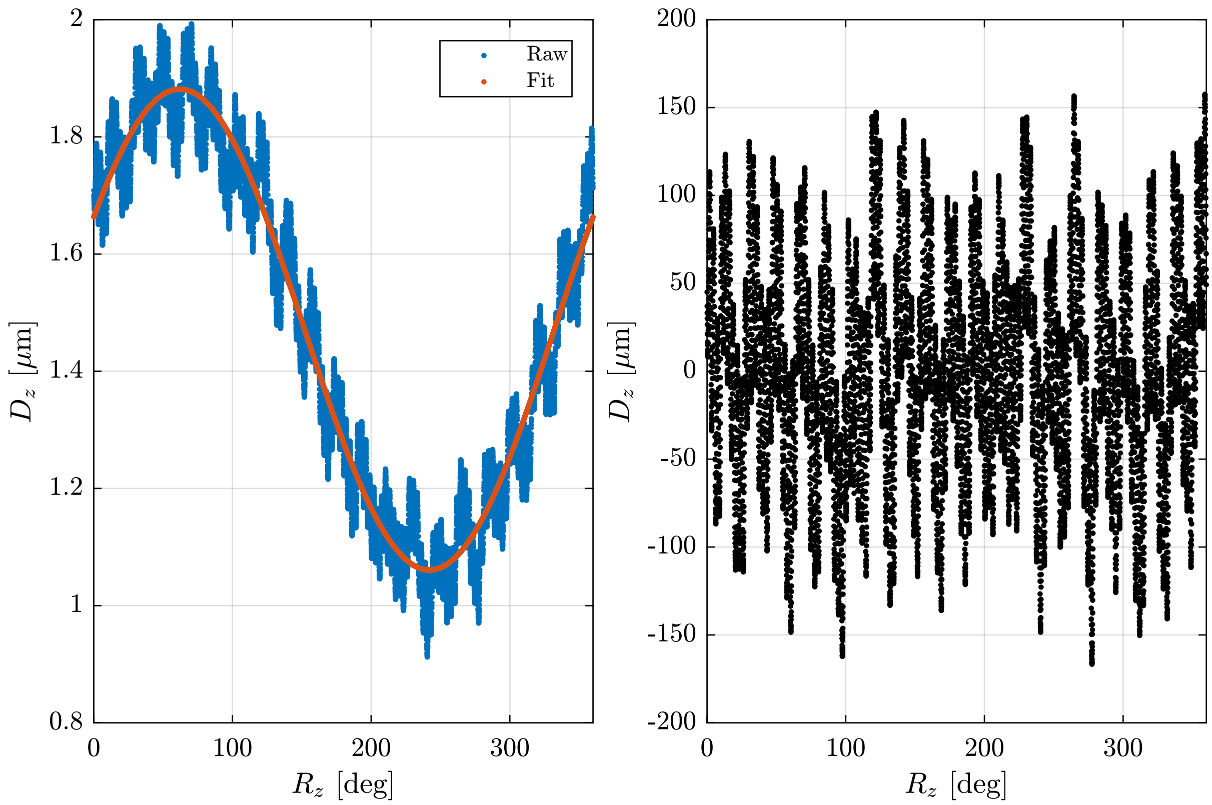

Figure 1.8: Effect of the excentricity and remaining Dz motion

```
Results
Errors linked to spindle motor = 58 [nm]
```

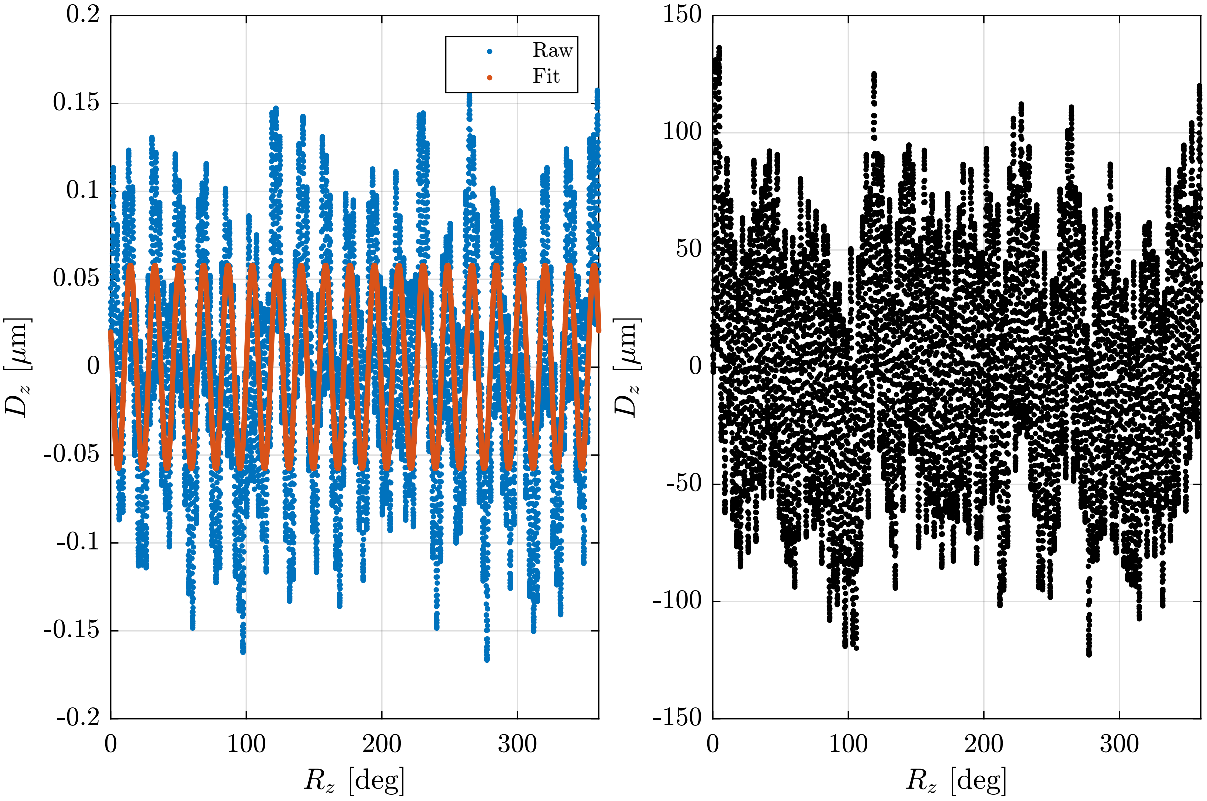

Figure 1.9: Effect of the magnetic pole pairs and remaining Dz motion

Let's look at the signal in the frequency domain.

On top of the peak at 1Hz (excentricity) and at 20Hz (number of pole pairs), we can observe a frequency of 126Hz (i.e. 126 periods per turn, approx 2.85 deg).

> ould this be related to the air bearing system?

1.3.3 Angle errors in R_x and R_y

```
Results
amplitude = 281 urad
```

Let's now analyse the frequency content in the signal.

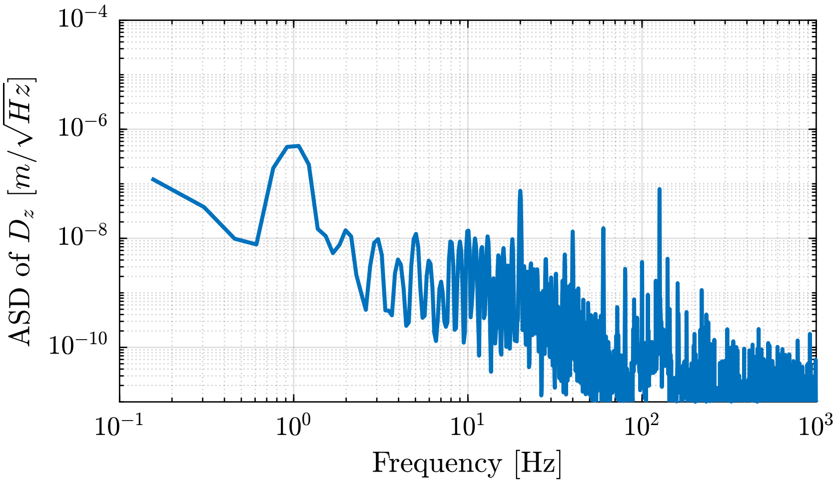

Figure 1.10: Amplitude Spectral Density of the measured Dz motion

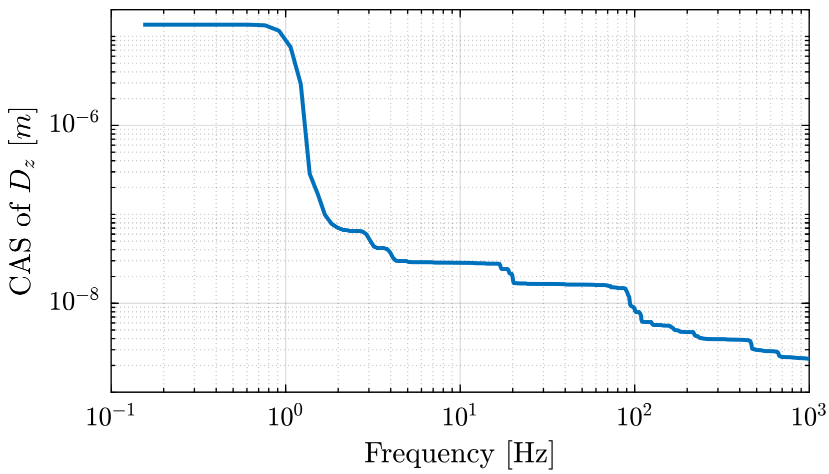

Figure 1.11: Cumulative Amplitude Spectrum of the measured Dz motion

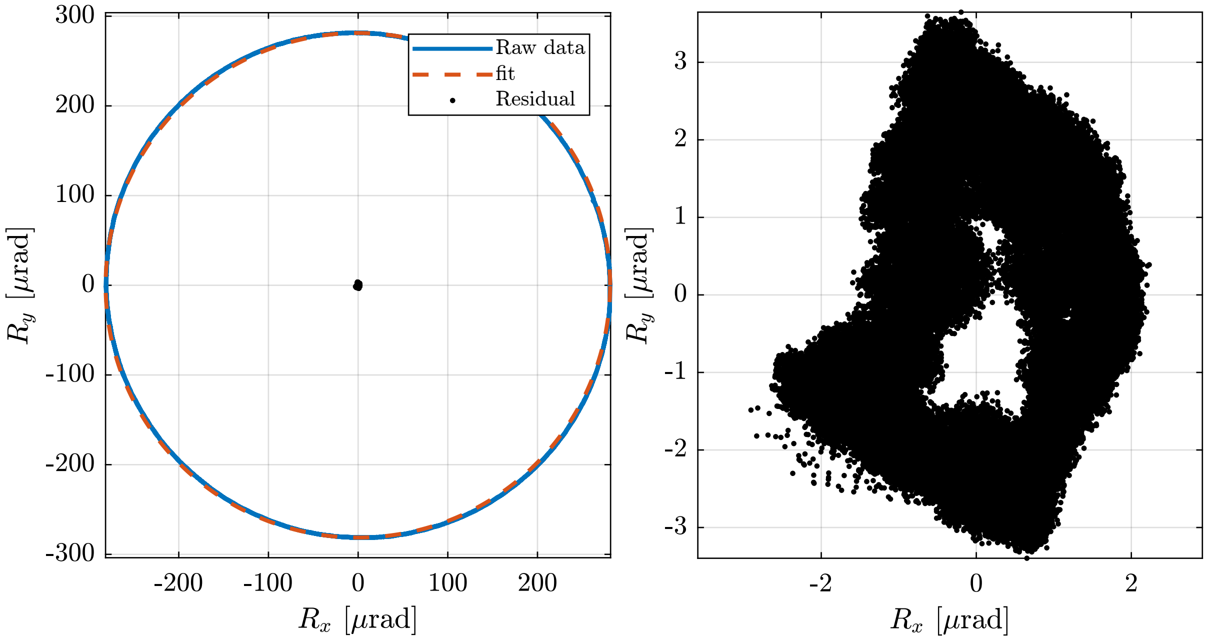

Figure 1.12: Rx and Ry motion during the spindle rotation

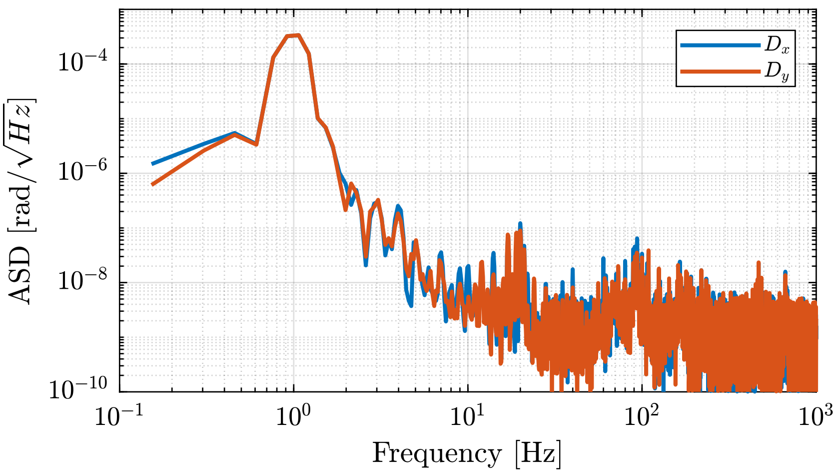

Figure 1.13: Amplitude Spectral Density of the measured Rx and Ry motion

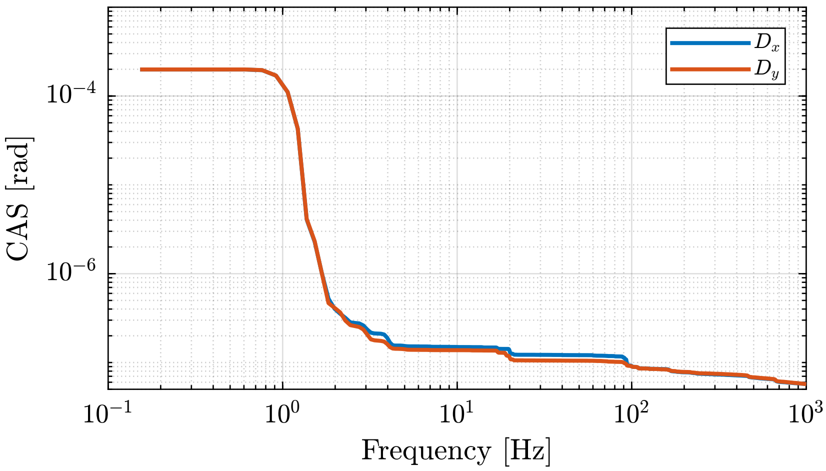

Figure 1.14: Cumulative Amplitude Spectrum of the measured Rx and Ry motion

2 Simscape Model

A 3D view of the Simscape model is shown in Figure 2.1. The Spindle is represented by a *Bushing joint*. Axial, radial and tilt stiffnesses are taken from the Spindle datasheet (see Table).

Table 2.1: Spindle stiffnesses

Stiffness	Value	Unit
Axial	402	$N/\mu m$
Radial	226	$N/\mu m$
Tilt	2380	$Nm/mrad$

The metrology system consists of 5 distance measurements (represented by the red lines in Figure 2.1).

2.1 Simscape model parameters

The nano-hexapod is initialized.

The Jacobian matrix that computes the $[x, y, z, R_x, R_y]$ motion of the sample from the 5 interferometers is defined below.

2.2 Control Architecture

Let's note:

- $d\mathcal{L}_m = [d_{\mathcal{L}_1},\ d_{\mathcal{L}_2},\ d_{\mathcal{L}_3},\ d_{\mathcal{L}_4},\ d_{\mathcal{L}_5},\ d_{\mathcal{L}_6}]$ the measurement of the 6 encoders fixed to the nano-hexapod
- $\boldsymbol{\tau}_m = [\tau_{m_1},\ \tau_{m_2},\ \tau_{m_3},\ \tau_{m_4},\ \tau_{m_5},\ \tau_{m_6}]$ the voltages measured by the 6 force sensors
- $\boldsymbol{u} = [u_1,\ u_2,\ u_3,\ u_4,\ u_5,\ u_6]$ the voltages send to the voltage amplifiers for the 6 piezoelectric actuators
- R_z the spindle measured angle (encoder)
- $\boldsymbol{d}_m = [d_1,\ d_2,\ d_3,\ d_4,\ d_5]$ the distances measured by the 5 interferometers (see Figure 2.2)

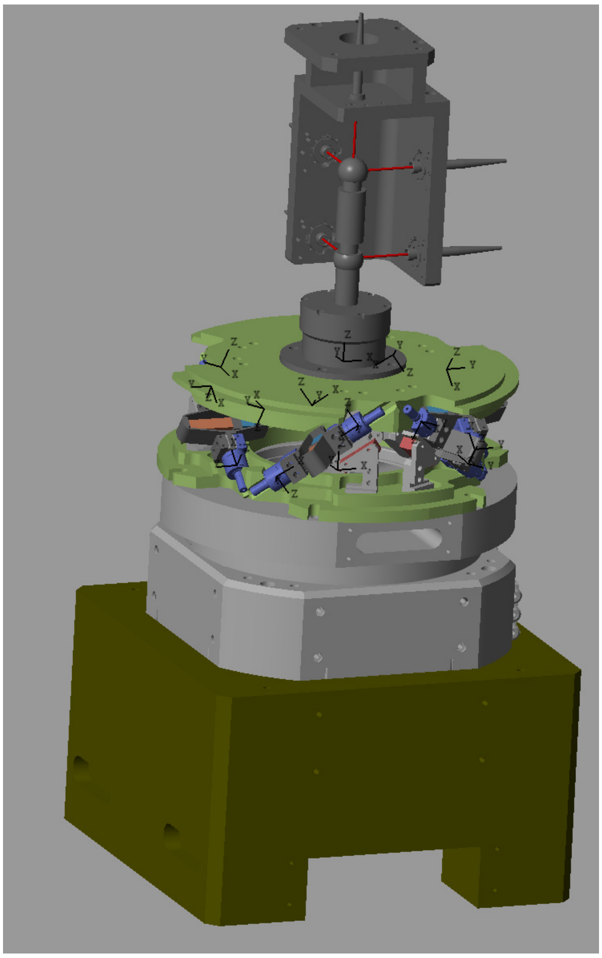

Figure 2.1: Screenshot of the 3D view of the Simscape model

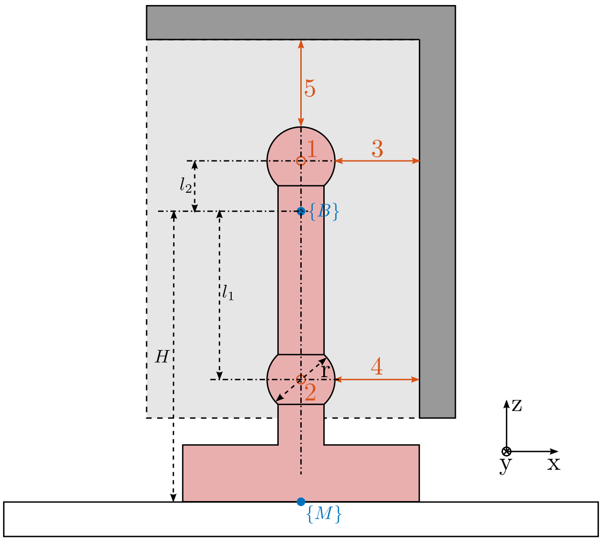

Figure 2.2: Schematic of the measurement system

2.3 Computation of the strut errors from the external metrology

The following frames are defined:

- $\{W\}$: the frame that represents the wanted pose of the sample
- $\{M\}$: the frame that represents the measured pose of the sample (estimated from the 5 interferometers and the spindle encoder)
- $\{G\}$: the frame fixed to the granite and positioned at the sample's center
- $\{H\}$: the frame fixed to the the spindle rotor, and positioned at the sample's center

We can express several homogeneous transformation matrices.

Frame fixed to the spindle rotor (centered on the sample's position), expressed in the frame of the granite:

$$ {}^G\boldsymbol{T}_H = \begin{bmatrix} cos(R_z) & -sin(R_z) & 0 & 0 \\ sin(R_z) & cos(R_z) & 0 & 0 \\ 0 & 0 & 1 & 0 \\ 0 & 0 & 0 & 1 \end{bmatrix} \tag{2.1} $$

with R_z the spindle encoder.

Wanted position expressed in the frame of the granite:

$$ {}^G\boldsymbol{T}_W = \begin{bmatrix} & & & r_{D_x} \\ & \boldsymbol{R}_x(r_{R_x})\boldsymbol{R}_y(r_{R_y})\boldsymbol{R}_z(r_{R_z}) & & r_{D_y} \\ & & & r_{D_z} \\ 0 & 0 & 0 & 1 \end{bmatrix} \tag{2.2} $$

with $\boldsymbol{R}(r_{R_x}, r_{R_y}, r_{R_z})$ representing the wanted orientation of the sample with respect to the granite. Typically, $r_{R_x} = 0$, $r_{R_y} = 0$ and r_{R_z} corresponds to the spindle encoder R_z.

Measured position of the sample with respect to the granite:

$$ {}^G\boldsymbol{T}_M = \begin{bmatrix} & & & y_{D_x} \\ & \boldsymbol{R}_x(y_{R_x})\boldsymbol{R}_y(y_{R_y})\boldsymbol{R}_z(R_z) & & y_{D_y} \\ & & & y_{D_z} \\ 0 & 0 & 0 & 1 \end{bmatrix} \tag{2.3} $$

with R_z the spindle encoder, and $[y_{D_x},\ y_{D_y},\ y_{D_z},\ y_{R_x},\ y_{R_y}]$ are obtained from the 5 interferometers:

$$ \begin{bmatrix} y_{D_x} \\ y_{D_y} \\ y_{D_z} \\ y_{R_x} \\ y_{R_y} \end{bmatrix} = \begin{bmatrix} 0 & -1 & 0 & l_2 & 0 \\ 0 & -1 & 0 & -l_1 & 0 \\ -1 & 0 & 0 & 0 & -l_2 \\ -1 & 0 & 0 & 0 & l_1 \\ 0 & 0 & -1 & 0 & 0 \end{bmatrix}^{-1} \cdot \begin{bmatrix} d_1 \\ d_2 \\ d_3 \\ d_4 \\ d_5 \end{bmatrix} \tag{2.4} $$

In order to have the **position error in the frame of the nano-hexapod**, we have to compute ${}^M\boldsymbol{T}_W$:

$$ {}^M\boldsymbol{T}_W = {}^M\boldsymbol{T}_G \cdot {}^G\boldsymbol{T}_W \tag{2.5} $$

$$ = {}^G\boldsymbol{T}_M{}^{-1} \cdot {}^G\boldsymbol{T}_W \tag{2.6} $$

The **inverse of the transformation matrix** can be obtained by

$$
{}^B\boldsymbol{T}_A = {}^A\boldsymbol{T}_B^{-1} = \left[\begin{array}{ccc|c} & {}^A\boldsymbol{R}_B^T & & -{}^A\boldsymbol{R}_B^T \, {}^A\boldsymbol{P}_{O_B} \\ \hline 0 & 0 & 0 & 1 \end{array} \right] \tag{2.7}
$$

The position errors $\boldsymbol{\epsilon}_{\mathcal{X}} = [\epsilon_{D_x},\ \epsilon_{D_y},\ \epsilon_{D_z},\ \epsilon_{R_x},\ \epsilon_{R_y},\ \epsilon_{R_z}]$ expressed in a frame fixed to the nano-hexapod can be extracted from ${}^W\boldsymbol{T}_M$:

- $\epsilon_{D_x} = {}^M\boldsymbol{T}_W(1,4)$
- $\epsilon_{D_y} = {}^M\boldsymbol{T}_W(2,4)$
- $\epsilon_{D_z} = {}^M\boldsymbol{T}_W(3,4)$
- $\epsilon_{R_y} = \text{atan2}({}^M\boldsymbol{T}_W(1,3), \sqrt{{}^M\boldsymbol{T}_W(1,1)^2 + {}^M\boldsymbol{T}_W(1,2)^2})$
- $\epsilon_{R_x} = \text{atan2}(\frac{-{}^M\boldsymbol{T}_W(2,3)}{\cos(\epsilon_{R_y})}, \frac{{}^M\boldsymbol{T}_W(3,3)}{\cos(\epsilon_{R_y})})$
- $\epsilon_{R_z} = \text{atan2}(\frac{-{}^M\boldsymbol{T}_W(1,2)}{\cos(\epsilon_{R_y})}, \frac{{}^M\boldsymbol{T}_W(1,1)}{\cos(\epsilon_{R_y})})$

Finally, the strut errors $\boldsymbol{\epsilon}_{\mathcal{L}} = [\epsilon_{L_1},\ \epsilon_{L_2},\ \epsilon_{L_3},\ \epsilon_{L_4},\ \epsilon_{L_5},\ \epsilon_{L_6}]$ can be computed from:

$$
\boldsymbol{\epsilon}_{\mathcal{L}} = \boldsymbol{J} \cdot \boldsymbol{\epsilon}_{\mathcal{X}} \tag{2.8}
$$

2.4 IFF Plant

2.5 DVF Plant

2.6 HAC Plant

The transfer functions from the 6 actuator inputs to the 6 estimated strut errors are extracted from the Simscape model.

The obtained transfer functions are shown in Figure 2.3.

We can see that the system is well decoupled at low frequency (i.e. below the first resonance of the Nano-Hexapod).

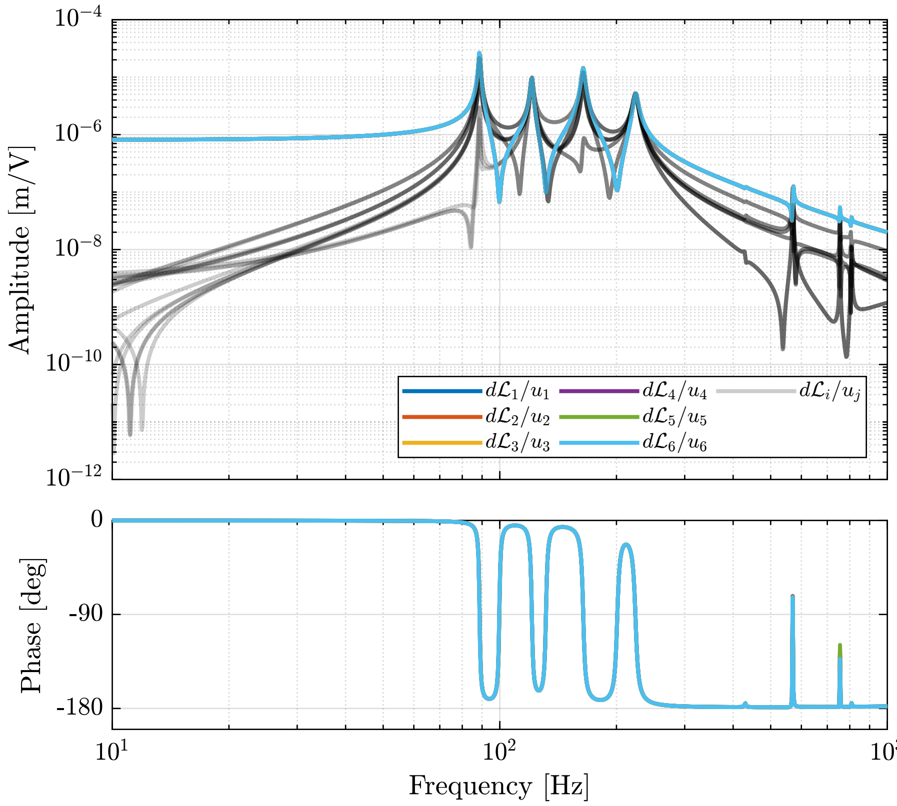

Figure 2.3: HAC plant obtained on the Simscape model

3 Control Experiment

3.1 IFF Plant

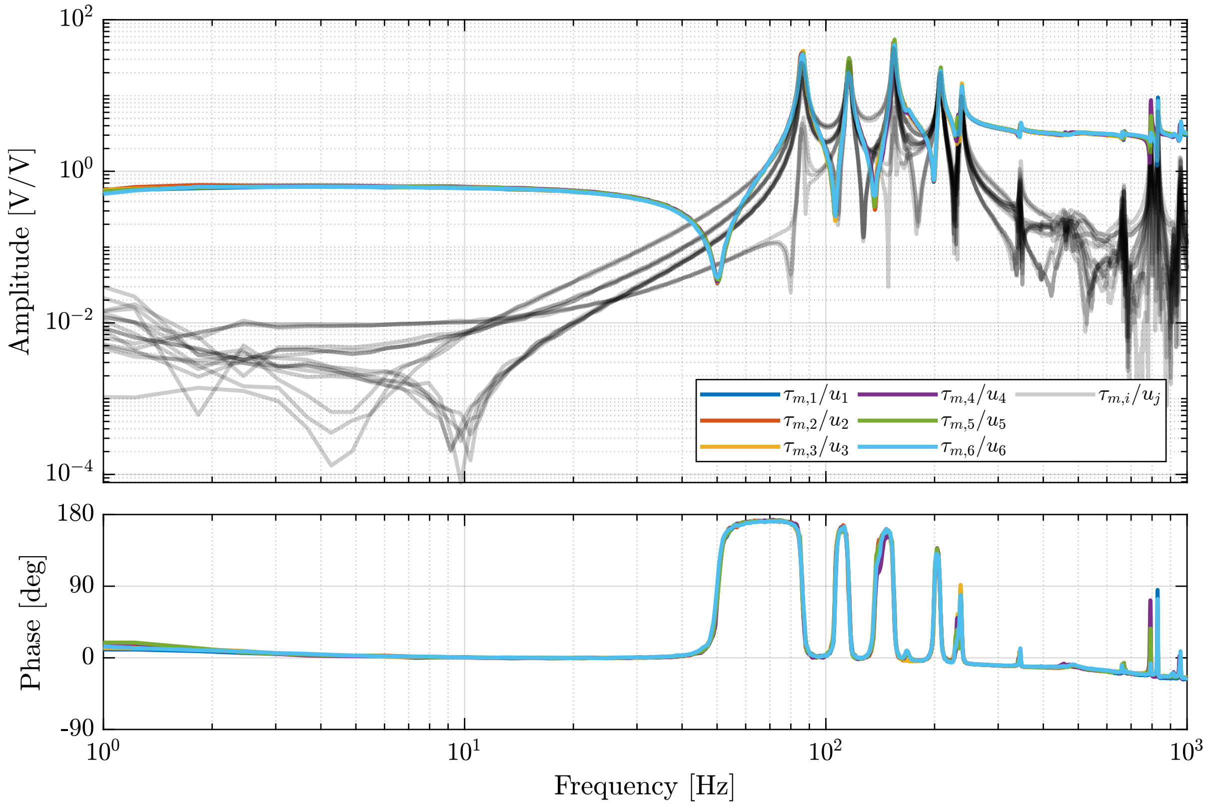

Figure 3.1: Obtained transfer function from generated voltages to measured voltages on the piezoelectric force sensor

3.2 IFF Controller

3.3 Open Loop Plant

Here the R_z motion of the Hexapod is estimated from the encoders.

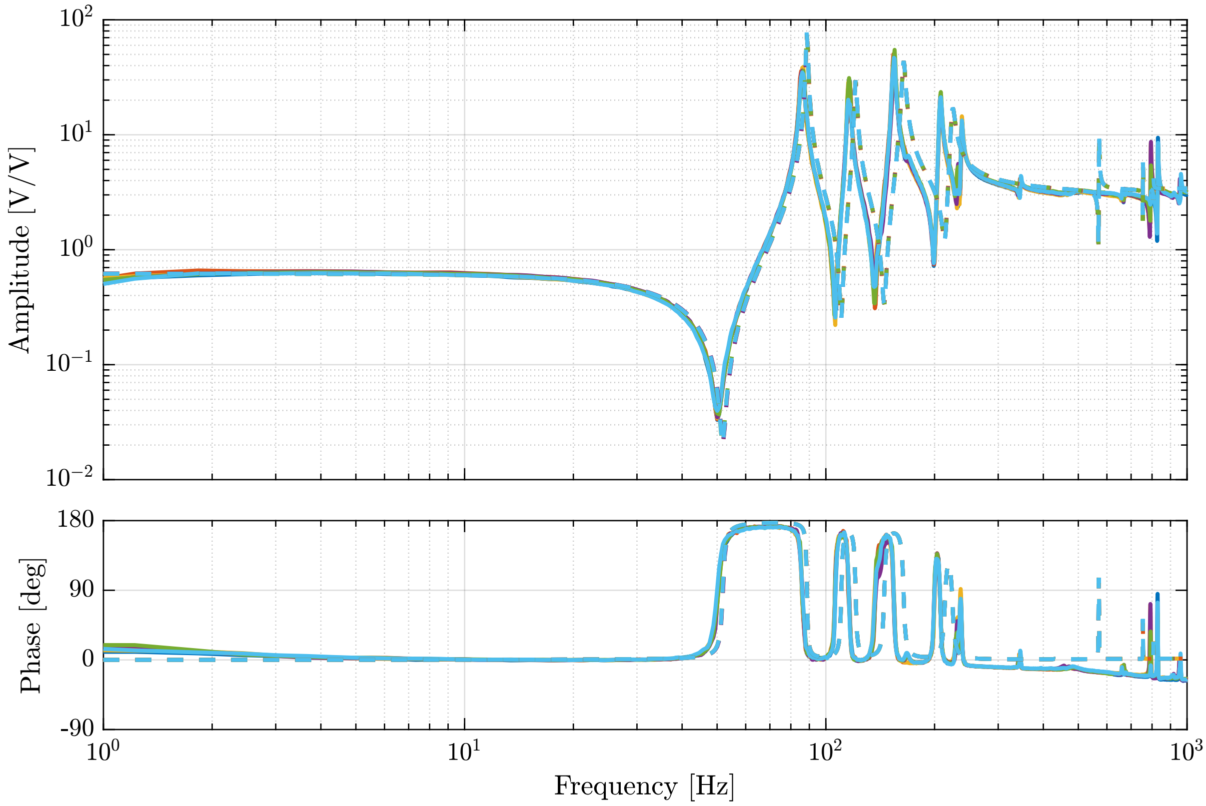

Figure 3.2: Comparison with the model

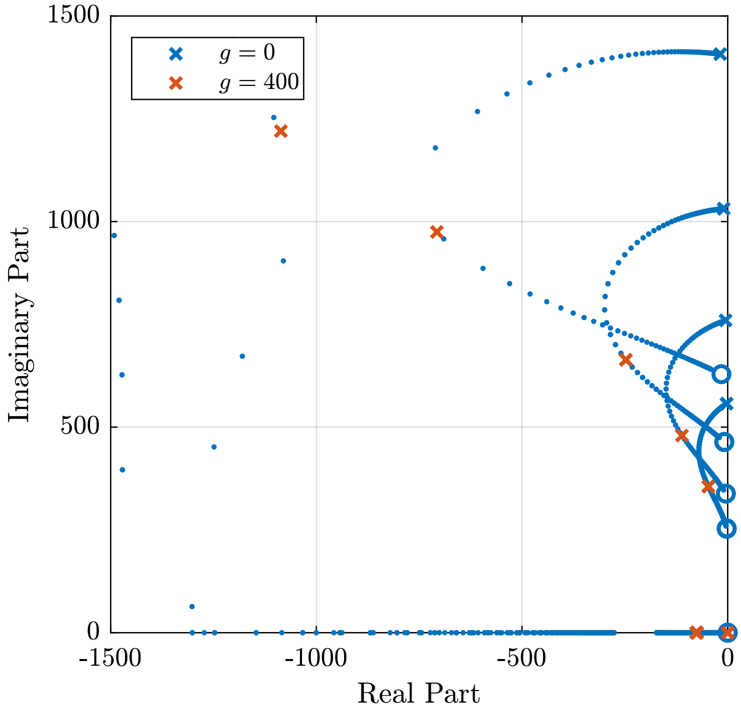

Figure 3.3: Root Locus for IFF

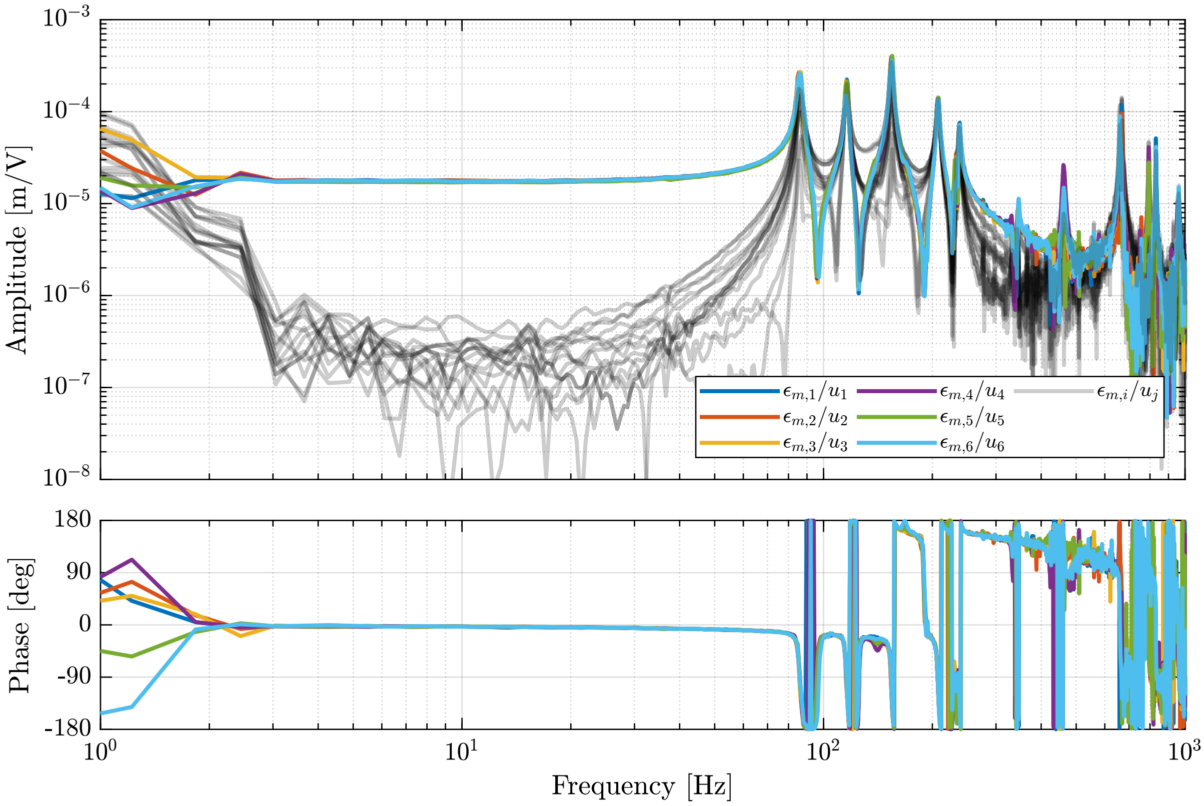

Figure 3.4: Obtained transfer function from generated voltages to estimated strut motion

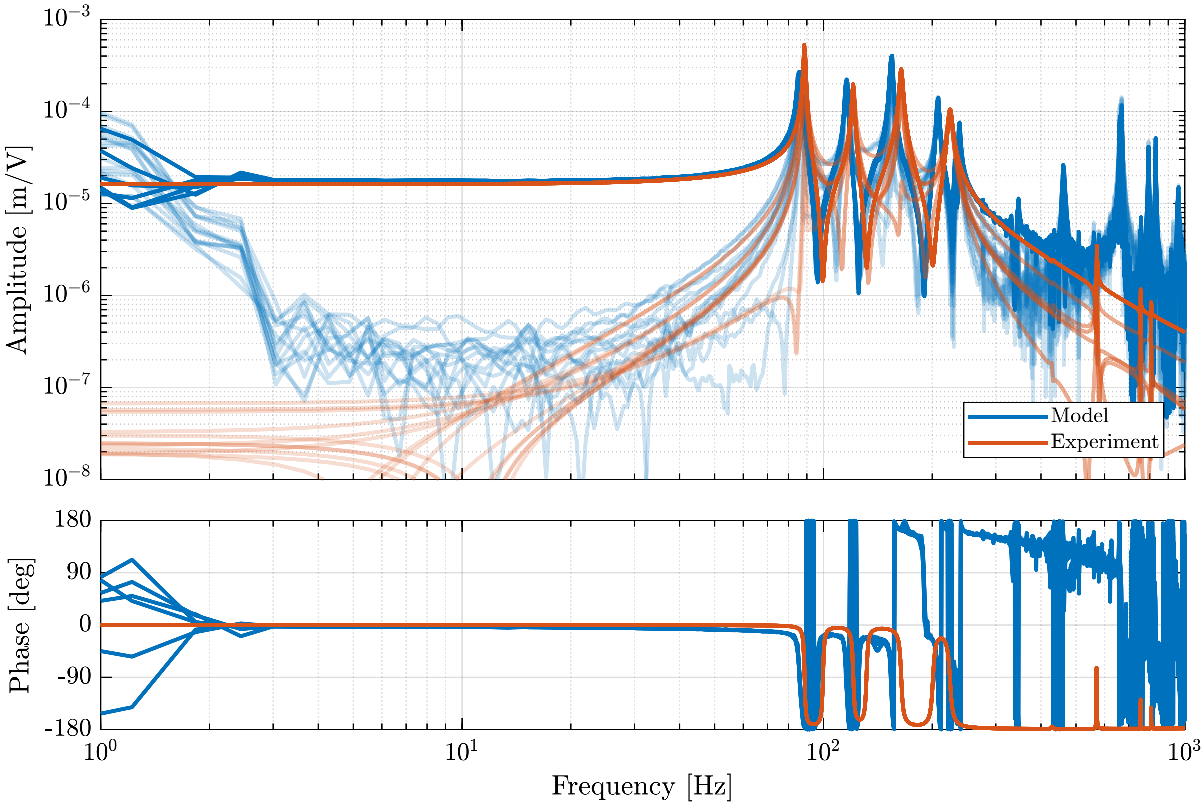

Figure 3.5: Comparison of the open-loop plant measured experimentally and extracted from Simscape

3.4 Damped Plant

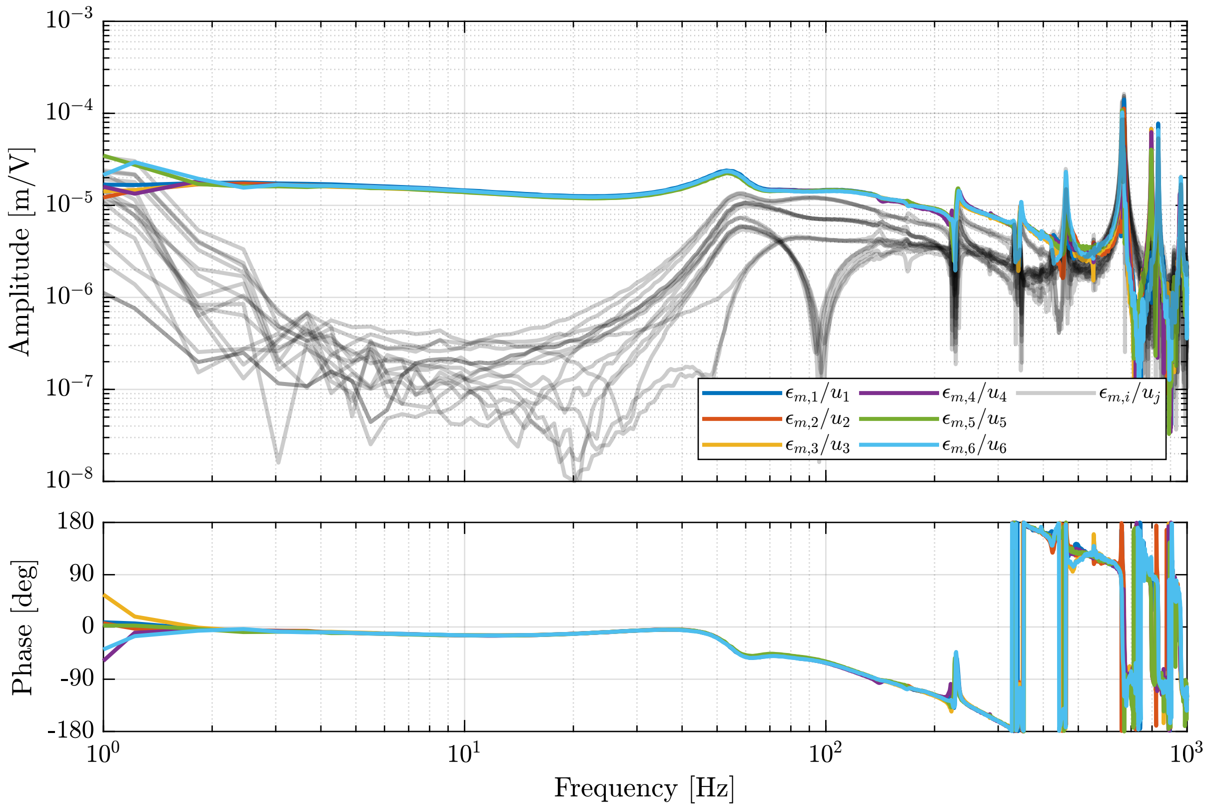

Figure 3.6: Obtained transfer function from generated voltages to estimated strut motion

3.5 HAC Controller

3.6 Compare dynamics seen by interferometers and by encoders

3.7 Compare dynamics obtained with different Rz estimations

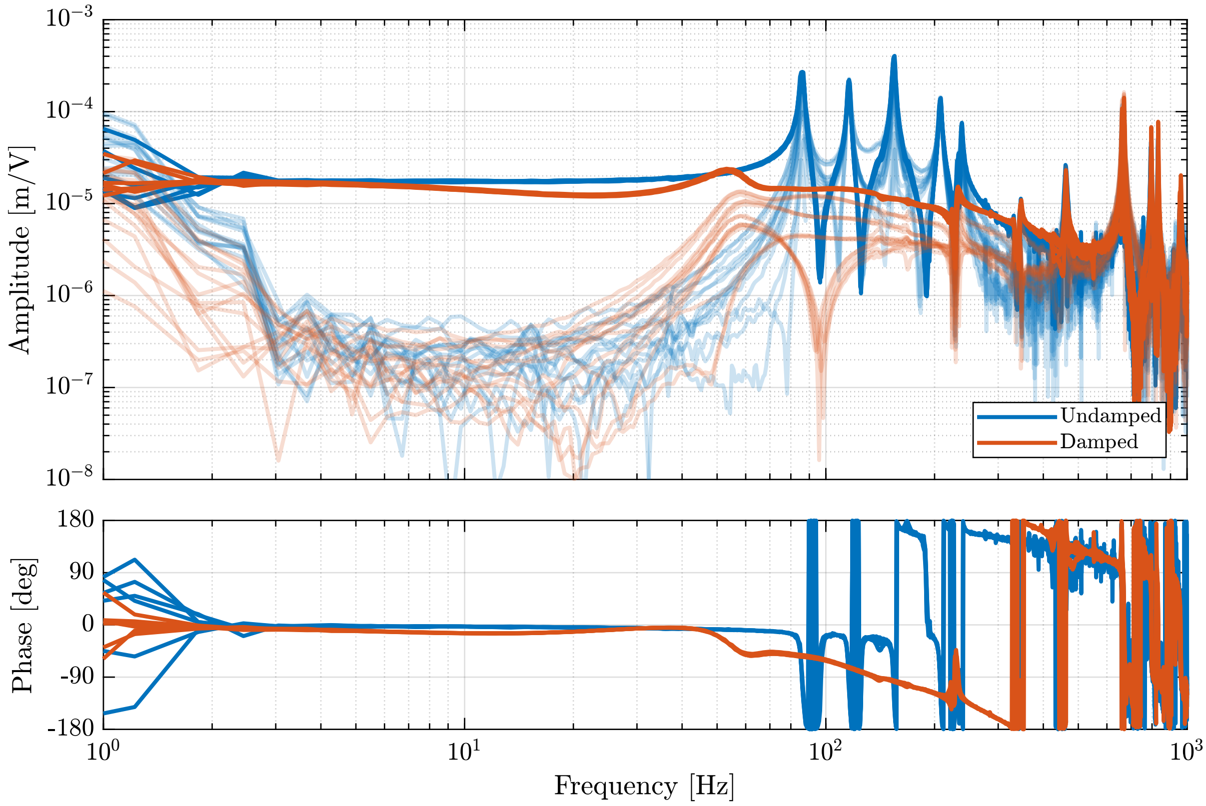

Figure 3.7: Comparison of the undamped and damped plant with IFF

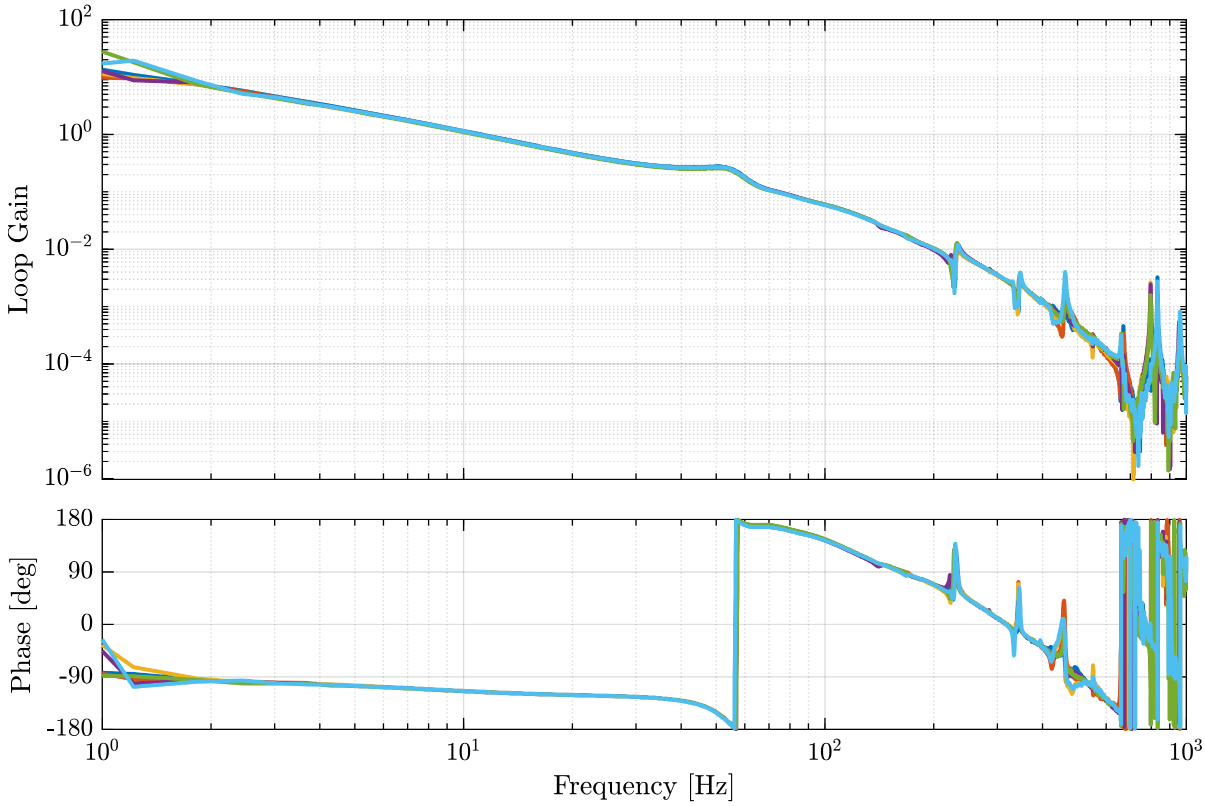

Figure 3.8: Loop gain for the HAC

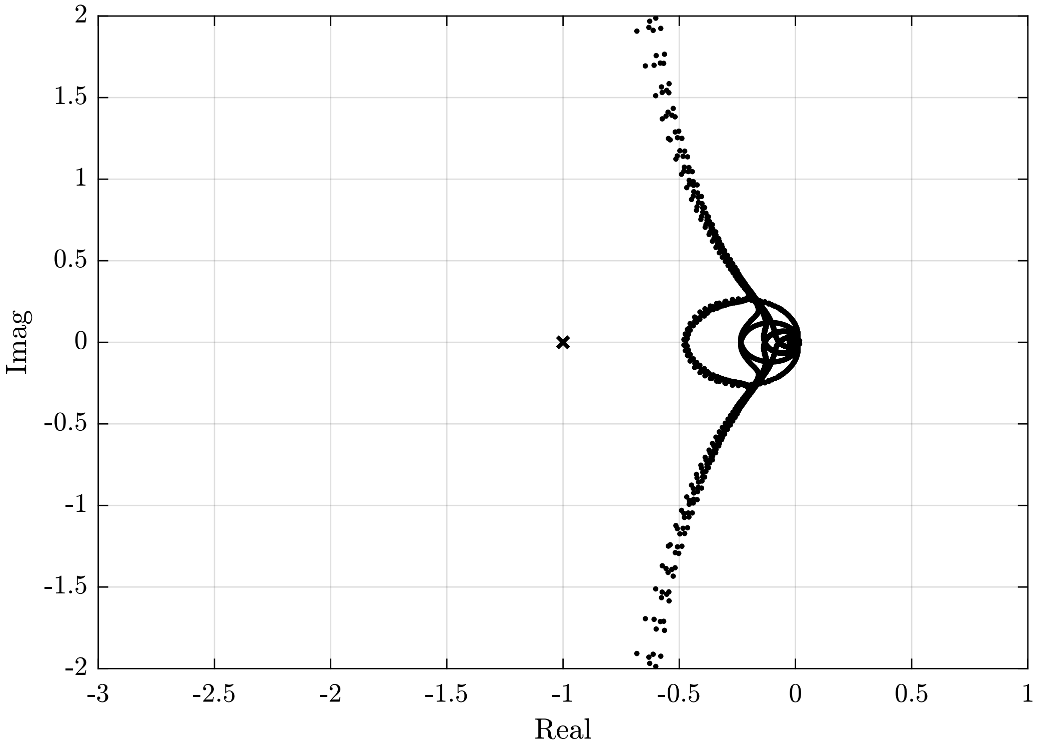

Figure 3.9: Obtained Root Locus

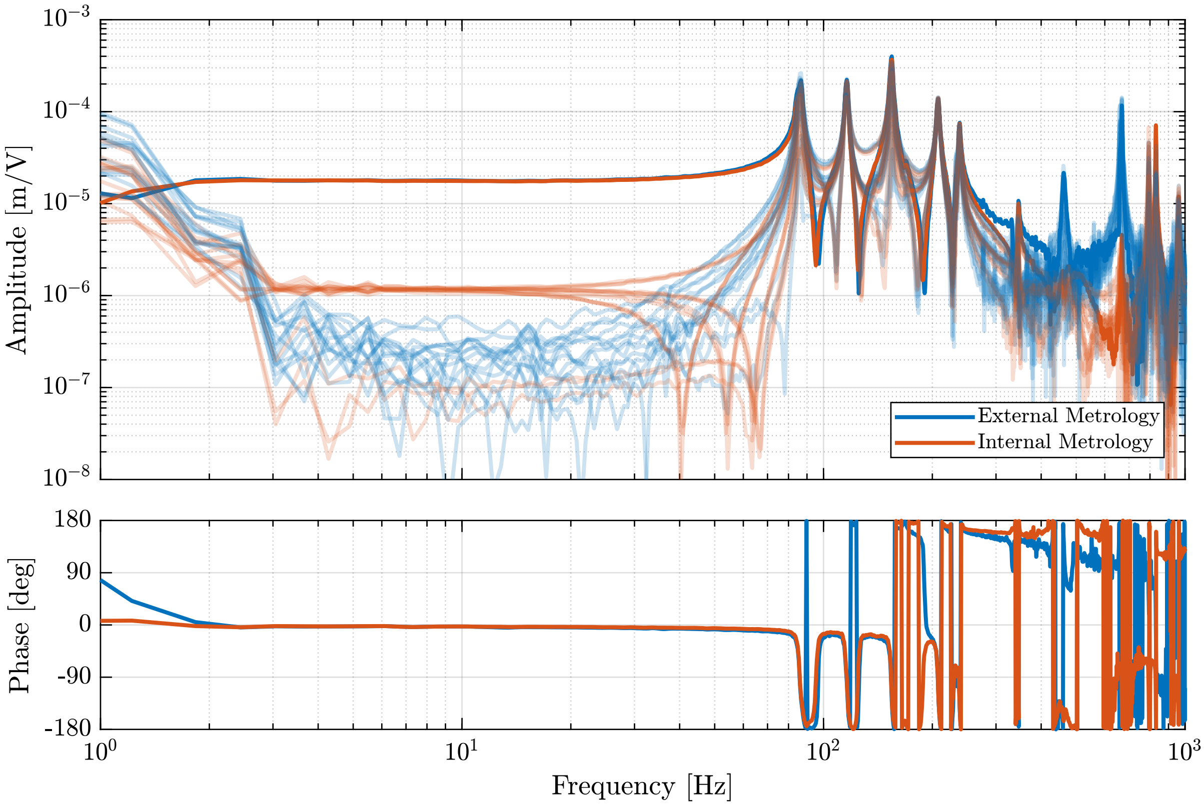

Figure 3.10: Comparison of the identified dynamic by the internal metrology (encoders) and by the external metrology (interferometers)

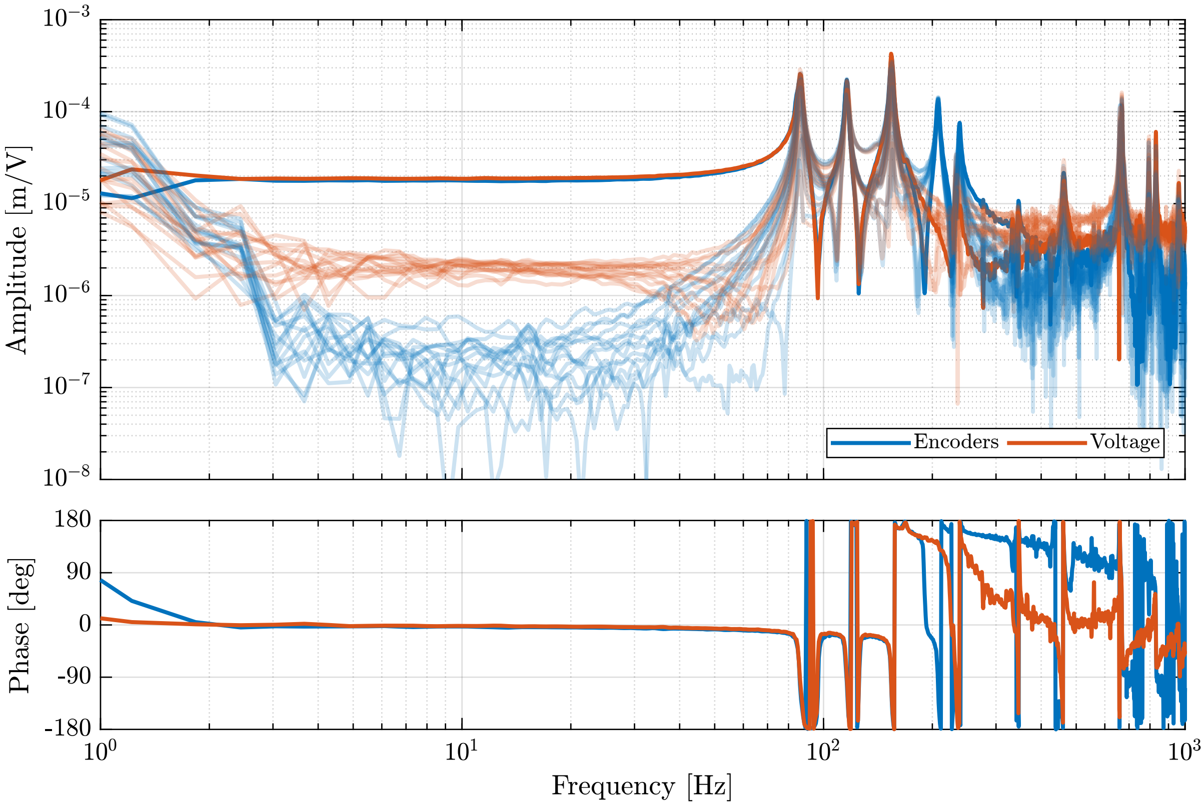

Figure 3.11: Comparison of the obtained plant using the Encoders or using the output Voltages to estimate Rz

4 Closed-Loop Results

4.1 Open and Closed loop results

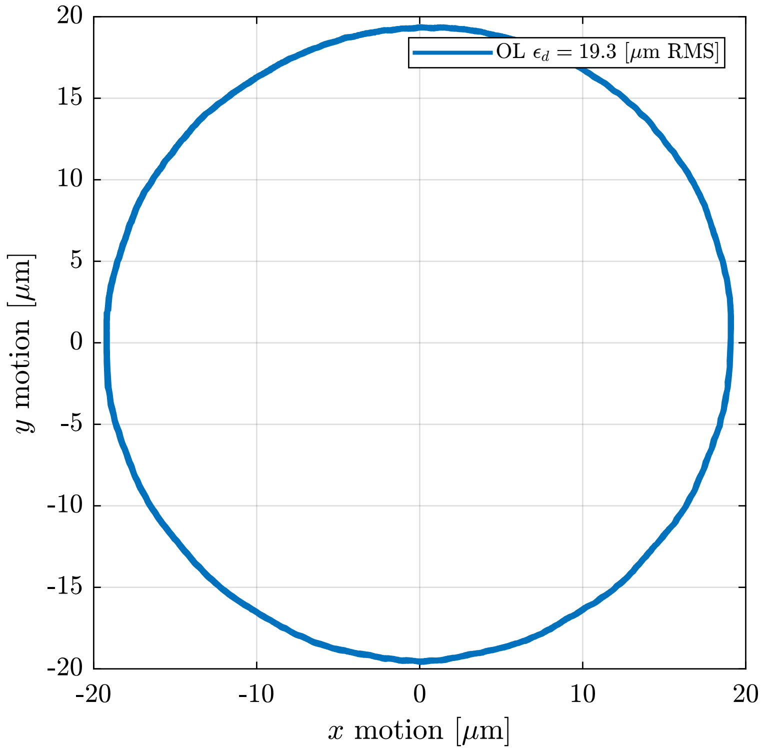

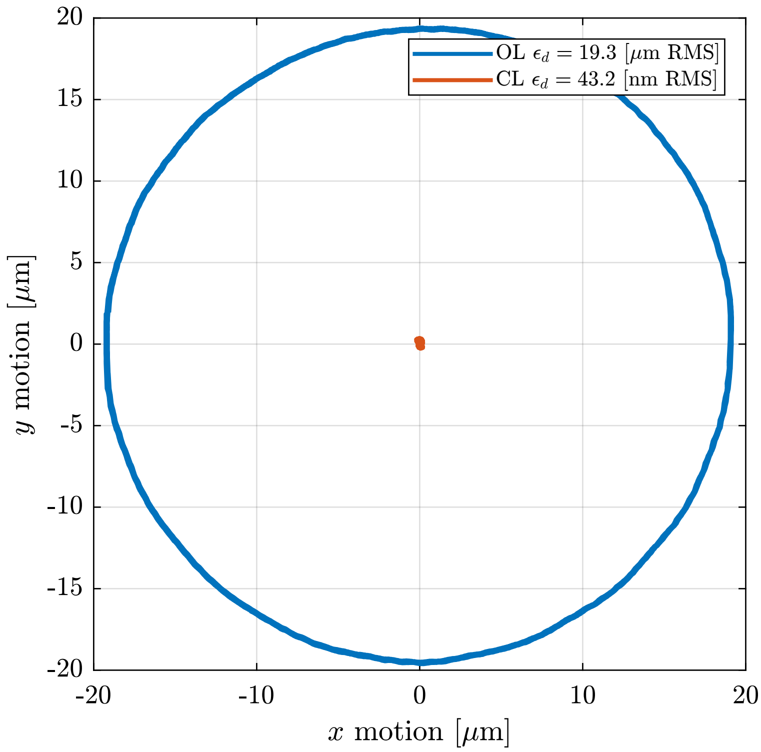

Figure 4.1: Comparison of the Open-Loop and Closed-Loop spindle errors

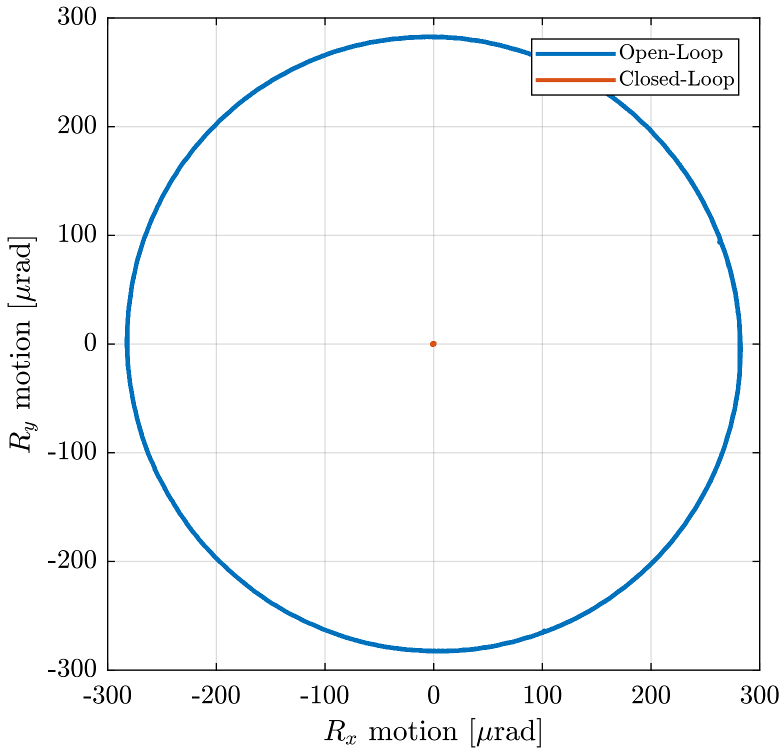

Figure 4.2: Comparison of the Open-Loop and Closed-Loop spindle errors - Rotation